

Net-Baryon Physics: Basic Mechanisms

J. Alvarez-Muñiz

IGFAE and Dep. Física Partículas, Univ. Santiago de Compostela, 15782 Santiago de Compostela, Spain

R. Conceição, J. Dias de Deus, M.C. Espírito Santo, J. G. Milhano, and M. Pimenta*

CENTRA, LIP and IST, Av. Rovisco Pais, 1049-001 Lisboa, Portugal

(Dated: September 25, 2021)

It is well known that, in nuclear collisions, a sizable fraction of the available energy is carried away by baryons. As the baryon number is conserved, the net-baryon $B - \bar{B}$ retains information on the energy-momentum carried by the incoming nuclei. A simple but consistent model for net-baryon production in high energy hadron-hadron, hadron-nucleus and nucleus-nucleus collisions is presented. The basic ingredients of the model are valence string formation based on standard PDFs with QCD evolution and string fragmentation via the Schwinger mechanism. The results of the model are presented and compared with both data and existing models. These results show that a good description of the main features of net-baryon data is possible on the framework of a simplistic model, with the advantage of making the fundamental production mechanisms manifest.

PACS numbers: 12.38.Aw, 12.39.-x, 12.40.Nn, 13.85.Ni, 24.85.+p

I. INTRODUCTION

In hadron-hadron, hadron-nucleus and nucleus-nucleus interactions a sizable fraction of the available energy in a collision is carried away by baryons [1, 2, 3]. As the baryon number is conserved, the measured net-baryon, $B - \bar{B}$, keeps track of the energy-momentum carried by the incoming particles. An important question to be asked is: how does the fraction of energy carried by the net-baryon evolve as a function of the centre-of-mass collisional energy per nucleon, \sqrt{s} ? This question is important because, on one hand, a decrease of the fraction of energy going into the net-baryon implies more energy available to create the deconfined quark-gluon state of matter, and on the other hand, such a decrease may reduce the possibility of producing fast particles in very high energy cosmic ray experiments. For more than 30 years, since the ISR at CERN, particle production studies have been limited to mid rapidity. Fortunately, with RHIC, large rapidity data became available, and, hopefully, the same will happen for the LHC. In fact, if one does not measure the physics at high rapidity the most elementary physical constraint, namely energy conservation, cannot be applied [4, 5].

In most of the existing Monte Carlo models [6, 7, 8, 9], the physics of net-baryon production is very much obscured by the complexity of extensive and detailed codes. Often, the basic production mechanisms do not appear in a transparent way. In this paper we present a simple but consistent model for net-baryon production in high energy hadron-hadron (h-h), hadron-nucleus (h-A) and nucleus-nucleus (A-A) collisions. As it happens in most of the existing codes, we shall work in the framework of the Dual Parton Model (DPM) [10] with string formation

(valence strings, in the present case) based on standard Parton Distribution Functions (PDFs) with QCD evolution and string fragmentation via the Schwinger mechanism. The basic ingredients of the model are:

- Formation of extended color fields or strings, making use of PDFs for valence quarks;
- Evolution with momentum transfer Q^2 , as a consequence of the QCD evolution of the PDF's;
- Fragmentation of each string with formation of a fast baryon (net-baryon) and other particles.

This paper is organized as follows. In section II, the predictions of current models and the available experimental data are briefly reviewed and compared. In section III, our simple net-baryon model is described. The results of the model are presented and compared with data and with existing models in section IV. A summary and brief conclusions are presented in section V.

II. CURRENT MODEL PREDICTIONS AND EXPERIMENTAL DATA

The data presently available on net-proton or net-baryon production is scarce. The most recent results are from RHIC [11]. These results are presented both in terms of net-baryon rapidity y and in terms of rapidity loss, defined as

$$\langle \delta y \rangle = y_p - \langle y \rangle, \quad (1)$$

where y_p is the beam rapidity and $\langle y \rangle$ is the mean net-baryon rapidity after the collision, given by

$$\langle y \rangle = \frac{2}{N_{part}} \int_0^{y_p} y \frac{dN_{B-\bar{B}}(y)}{dy} dy. \quad (2)$$

*Corresponding author, pimenta@lip.pt

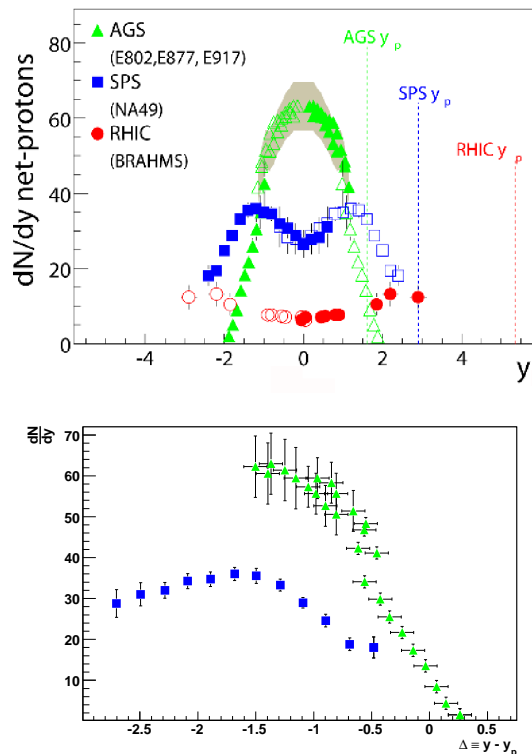


FIG. 1: The net-proton distribution at AGS [13] (Au+Au at $\sqrt{s} \approx 5$ GeV), SPS [14] (Pb+Pb at $\sqrt{s} \approx 17$ GeV), and RHIC (Au+Au at $\sqrt{s} = 200$ GeV) is shown (upper plot). The data correspond to the 5% most central collisions and the errors are both statistical and systematic (the light gray band shows the 10% overall normalization uncertainty on the E802 points, but not the 15% for E917). The data have been symmetrised. For RHIC data, filled points are measured and open points are symmetrised, while the opposite is true for AGS and SPS data (for clarity). At AGS weak decay corrections are negligible and at SPS they have been applied. Taken from [11]. The distribution of $\Delta \equiv y - y_p$ is shown (lower plot) for SPS and AGS data.

Here, N_{part} is the number of participants in the collision and $N_{B-\bar{B}}$ is the net-baryon number. It is worth noting that the net-baryon results depend directly on the number of participants in the collision and thus on the collision centrality. The relation between the number of participants and the impact parameter of the collision can be established, for instance, in the context of the Glauber model [12].

The net-baryon rapidity distributions at different centre-of-mass energies for different beam-target systems were compared in [11]. In figure 1, the net-proton distributions at AGS (Au+Au at $\sqrt{s} \approx 5$ GeV) [13], SPS (Pb+Pb at $\sqrt{s} \approx 17$ GeV) [14], and RHIC (Au+Au at $\sqrt{s} = 200$ GeV) [11] for central collisions (the 5% most central) are shown (upper plot). The distributions show a strong energy dependence, with the mid rapidity region corresponding to a peak at AGS, a dip at the SPS, and a broad minimum at RHIC. The distribution of $\Delta = y - y_p$

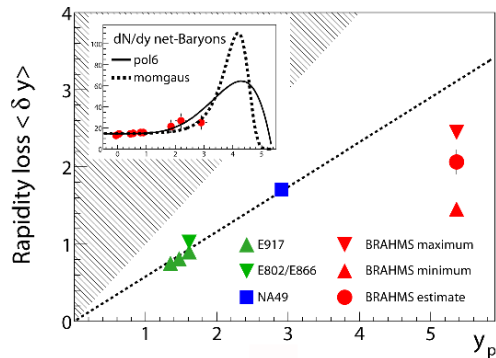


FIG. 2: Rapidity loss as a function of beam rapidity (in the CM). The hatched area indicates the unphysical region, and the dashed line shows the phenomenological scaling $\langle \delta y \rangle = 0.58 y_p$. The inset plot shows the BRAHMS net-baryon distribution (data points) with fits (lines) needed to extrapolate up to the beam rapidity, explaining the large uncertainty associated to the BRAHMS rapidity loss measurement. Taken from [11].

is shown (lower plot) for SPS and AGS data. It is apparent that neither Feynman scaling nor limiting fragmentation are satisfied in net-baryon production.

In figure 2, the rapidity loss data is shown as a function of the beam rapidity (in the centre-of-mass frame) for AGS, SPS and RHIC. The large uncertainty associated with the BRAHMS data point is, as illustrated in the inset plot, related to a relatively unconstrained extrapolation to the high rapidity region, required for the rapidity loss calculation.

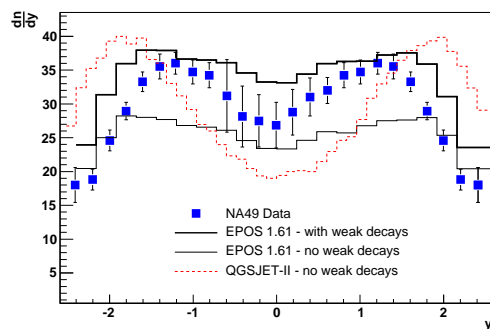


FIG. 3: The net-proton rapidity distributions from EPOS 1.61 (full lines) and QGSJET-II.03 (dashed line) for Pb-Pb collisions at $\sqrt{s} \approx 17$ GeV are shown and compared with data NA49 SPS data (points). For EPOS, the results obtained including (thick line) and excluding (thin line) the strangeness contribution are shown. For QGSJET, the “no-decays” curve is shown. For details on the data see figure 1

Let us now turn to net-baryon production as implemented in the existing Monte Carlo models. QGSJET-II [7] and EPOS [8] are amongst the presently most widely used hadronic models in high energy and cosmic ray physics. To our knowledge, there is no systematic study comparing the predictions of these two models on net-baryon production between themselves or with experimental data.

In figure 3, net-proton rapidity distributions obtained with QGSJET-II.03 and EPOS 1.61 for Pb-Pb collisions at $\sqrt{s} \simeq 17$ GeV are shown and compared with experimental data. According to [14] weak decay corrections have been applied to the data. Following [15], the impact parameter range (0 to 3.1 fm) corresponding to the centrality cut of 5% applied to data was selected in QGSJET and EPOS. For EPOS, the results obtained leaving all particles free to decay and contribute to the net-baryon are shown together with those obtained switching off all weak decays. The “all-decays” EPOS curve reproduces the trend seen in data, with an excess that could be due to the presence of net-baryon from weak decays. However, the strangeness effect compensation in the “no-decays” curve seems to be too strong. For QGSJET-II, the “no-decays” curve is shown (and was found to be very similar to what is obtained from the model by default). One should recall that QGSJET-II is not expected to perform very well at such low energies.

III. THE MODEL

Let us now describe a simple model for net-baryon production. In the spirit of [2, 3, 10, 16], the basic assumption is that net-baryon production in proton-proton collisions is strongly correlated with the formation and fragmentation of two color singlet strings, each one with two valence quarks from one of the protons, and one valence quark from the other proton. This is schematically shown in figure 4.

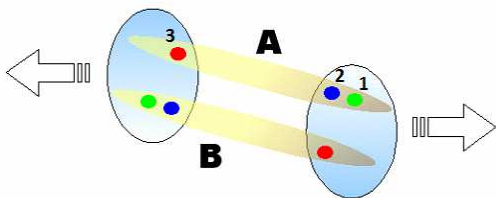


FIG. 4: Schematic representation of a proton-proton collision, with the formation of two valence strings.

Referring to the figure, let x_1 , x_2 and x_3 be the fractions of momentum carried by the valence quarks forming string A. Quarks 1 and 2 are from the proton with positive momentum in the proton-proton reference frame, and quark 3 is from the other proton. No transverse

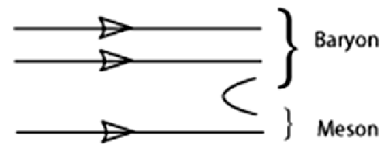


Diagram 1

$$x_1 - x_2 < x_2 - (-x_3)$$

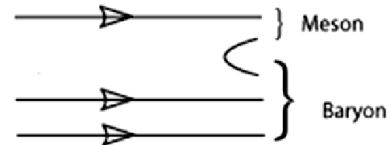


Diagram 2

$$x_1 - x_2 < x_2 - (-x_3)$$

FIG. 5: The two main valence string fragmentation diagrams.

momentum is considered within this model. By choice, $x_1 > x_2 > x_3$, with $x_3 < 0$. The energy and momentum of each string are obtained adding directly the energy and momentum carried by each of the valence quarks. For string A

$$E_{string} = (x_1 + x_2 + (-x_3)) \frac{\sqrt{s}}{2}, \quad (3)$$

$$P_{string} = (x_1 + x_2 - (-x_3)) \frac{\sqrt{s}}{2}, \quad (4)$$

$$M_{string} = \sqrt{(x_1 + x_2) (-x_3) s}, \quad (5)$$

where the momentum fractions x_1 , x_2 and x_3 are determined using the quark PDFs. For each \sqrt{s} , an effective momentum transfer Q^2 adjusted from experimental data was chosen (see section IV for details). In this work the CTEQ6M parton distribution functions [17] were used.

The simplest possible model for fragmentation is assumed. Each string decays into a baryon and a meson in the following way: the string is cut in two pieces and a $q\bar{q}$ pair is formed, from the vacuum, either between quarks 2 and 3 (belonging the different protons) or between quarks 1 and 2 (belonging to the same proton, with positive momentum in this string A example). The quark pair with the largest momentum difference is chosen. The string piece that inherits two valence quarks originates the baryon, whereas the string piece that inherits one valence quark originates the meson. This mechanism corresponds to the diagrams represented in figure 5. The weights of the two diagrams are, in this simple model, given only by kinematics. For string A the first diagram will be more probable (especially for low \sqrt{s}). However,

the weight of the second diagram can be as large as 40% above LHC energies.

The $q\bar{q}$ pair formed from the vacuum was taken to be either a $u\bar{u}$ or a $d\bar{d}$, and the full quark combinatorics was then performed in order to determine the nature of the possible outgoing baryon. Both fundamental and excited states were considered, taking spin-dependent weights $(2j+1)$. The decays of the unstable baryons were then performed and the outgoing nucleons included in the net-baryon calculations. The contribution from s quarks was not considered here. It was estimated from the Schwinger model to be about 25%.

The string mass and momentum distributions as function of Q^2 are given in figure 6. The mass distribution applies to both valence strings, while the momentum distribution for the case of string B is simply symmetric. The net-baryon rapidity distributions for different values of Q^2 are presented in figure 7, for two different centre-of-mass energies. This figure illustrates not only the evolution with Q^2 but also the clear effect of kinematics, due to the increase of \sqrt{s} , on the main features of the distribution.

It is worth noting that the inclusion of diagram 2, in addition to diagram 1, with weights determined simply by kinematics, reproduces some of the effects predicted in models with string junctions [18, 19] or popcorn [20] mechanisms for the transport of baryon number from the beam rapidity into the central region $y \sim 0$. These effects can thus be achieved in a simple DPM model, based on valence strings and a Q^2 parameterisation.

For the purpose of estimating the net-baryon production in A-A collisions, we shall use the simple approximation that $dn/dy(B - \bar{B})$ at a given \sqrt{s} is proportional to the number of participating nucleons, N_{part} ,

$$\frac{dn}{dy}\Big|_{A-A} \simeq \frac{1}{2} N_{part} \times \frac{dn}{dy}\Big|_{p-p}. \quad (6)$$

This relation is presumably reasonable as net-baryon production is originated from valence strings associated to wounded (or participating) nucleons. At mid rapidity, saturation effects originate additional production of mesons and baryons. This affects $(B + \bar{B})$, but not $B - \bar{B}$ production. An attempt to estimate nuclear effects correction factors for the valence quark PDFs was made using EKS98 [21] and nDS [22]. Values below 10-15% were found.

IV. RESULTS

In order to fully define the model, we need to choose an effective Q^2 value as input for the quark PDFs. This is done by adjusting the results of the model to the experimental data, i.e., by choosing, for each \sqrt{s} , the effective Q^2 for which the model better describes the data. In the fitting procedure, the global normalisation factor (the number of participants, relying on the approach of

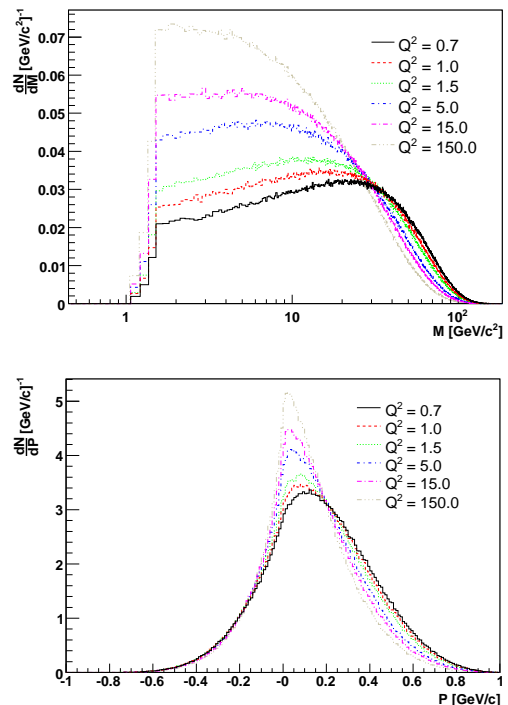


FIG. 6: Evolution with Q^2 of the string mass (upper plot) and momentum (lower plot) distributions for $\sqrt{s} = 200$ GeV. The mass distribution applies to both valence strings, while the momentum distribution for the case of string B is simply symmetric.

\sqrt{s} (GeV)	Collision	Q^2	N_{part}
5	Au-Au	$0.36^{+0.10}_{-0.01}$	260 ± 20
17	Pb-Pb	$0.64^{+0.17}_{-0.17}$	300 ± 20
200	Au-Au	$1.69^{+0.52}_{-0.78}$	280 ± 20

TABLE I: Results of the fit to the effective Q^2 and the number of participants at the different centre-of-mass energies.

eq. (6) is left as a second free parameter. In order to compare the results of this model on net-baryon to the experimental data on net-proton, we consider that net-proton is roughly 1/2 of $(B - \bar{B})$.

Figure 8 illustrates, for a specific \sqrt{s} and fixing the number of participants, the ability of the model to generate very different net-proton rapidity distributions, simply by choosing different values of the effective Q^2 . At $\sqrt{s} = 200$ GeV and $\sqrt{s} \simeq 17$ GeV all the data points (see figure 1) were included in the fit. At $\sqrt{s} \simeq 5$ GeV, and due to energy conservation constraints imposed in the model, only the points up to the nominal beam rapidity were considered.

The values obtained for the effective Q^2 and the number of participants N_{part} at the different centre-of-mass energies are given in table I.

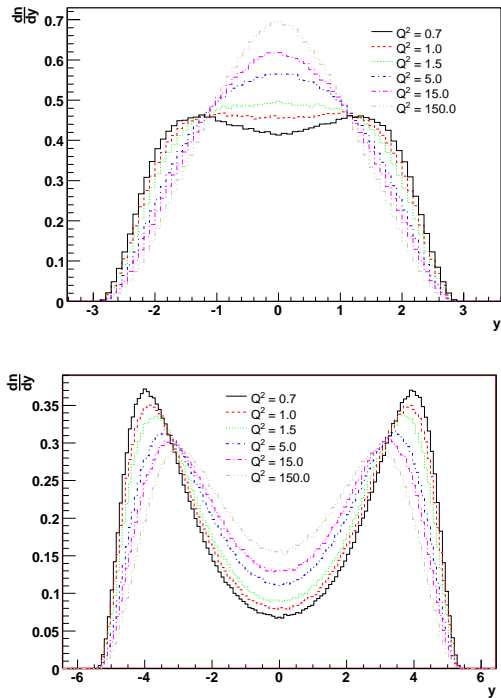


FIG. 7: Evolution of the net-baryon rapidity with Q^2 at $\sqrt{s} = 17$ GeV (upper plot) and $\sqrt{s} = 200$ GeV (lower plot).

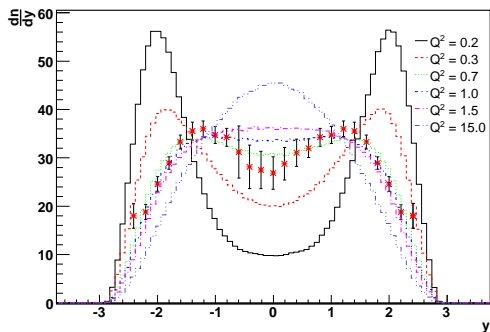


FIG. 8: Net-baryon predictions of the present model for different values of Q^2 , and comparison with data, at $\sqrt{s} \simeq 17$ GeV.

It is worth noting that the fitted N_{part} values are roughly compatible with what is expected from the literature, although about 20% lower. In fact, the average number of participants for Pb-Pb collisions at SPS energies is given in [15] as 362. Concerning Au-Au collisions, the value is expected to be only slightly lower (estimated as 344 to 357 at RHIC energies [11, 23, 24]) and expected to depend weakly on \sqrt{s} , in fair agreement with the obtained results. As pointed out in section III, in this simple model strangeness contribution to the net-baryon was not considered, and it amounts to about 25%, accounting for the

values obtained for the number of participants.

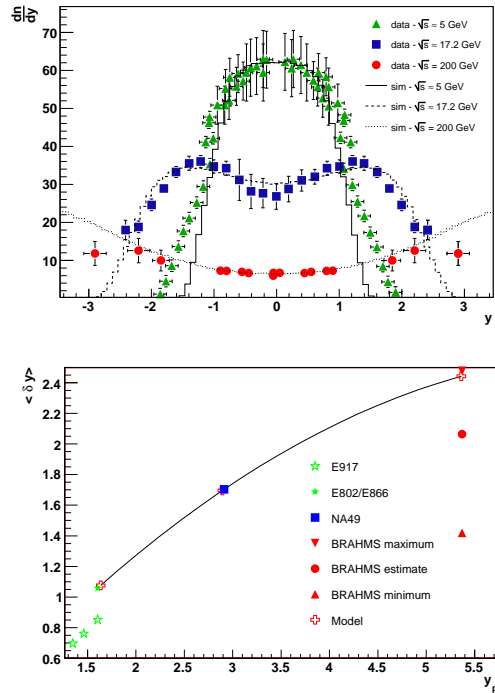


FIG. 9: The results of the present model for net-baryon rapidity (upper plot) and rapidity loss (lower plot) are compared to experimental data at different centre-of-mass energies. See figure 1 for details on the data points.

Figure 9 shows the results of the present model for net-baryon rapidity distribution and rapidity loss, in comparison with experimental data at different centre-of-mass energies. A fair agreement is found at the measured energies. For the lowest \sqrt{s} , the points above the nominal beam rapidity were not considered in the fit.

We can now try to find a relation between the effective Q^2 and \sqrt{s} . The effective Q^2 corresponds to the typical transverse size (area) of the parton (here, the valence quark). It is reasonable to assume, as in Regge phenomenology [25], that the average number of partons in a nucleon increases as a power of the centre of mass energy \sqrt{s} . Thus, $\sqrt{s}/Q^2 \sim R_h^2$, where R_h is the nucleon radius which we take as fixed. It then follows that Q^2 should grow according to

$$Q^2 = Q_0^2 \left(\frac{\sqrt{s}}{\sqrt{s_0}} \right)^{\lambda_v} [GeV^2]. \quad (7)$$

The exponent λ_v was determined by fitting eq. (7) to the available data points in table I.

The results are shown in figure 10, where the data points are the Q^2 values adjusted above, the line is the fit with eq. (7) and the shaded areas correspond to 1σ

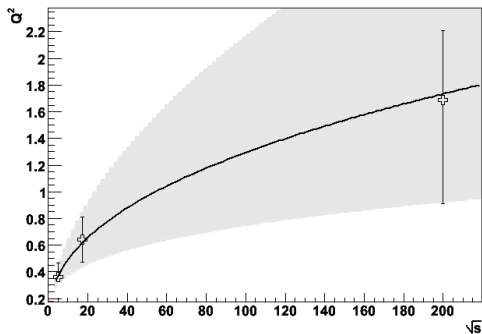


FIG. 10: The effective Q^2 values at different centre-of-mass energies chosen by tuning the model to the experimental data are shown. The line shows the fit to the points using eq. (7) and the shaded areas correspond to 1σ variations of the fit parameters.

variations of the fit parameters. The obtained results are $\lambda_v = 0.42^{+0.065}_{-0.120}$ and $Q_0^2 = 0.36^{+0.070}_{-0.015}$, taking $\sqrt{s_0} = 5$ GeV. It should however be noted that we have just three points in the fit and the 1σ band is rather wide.

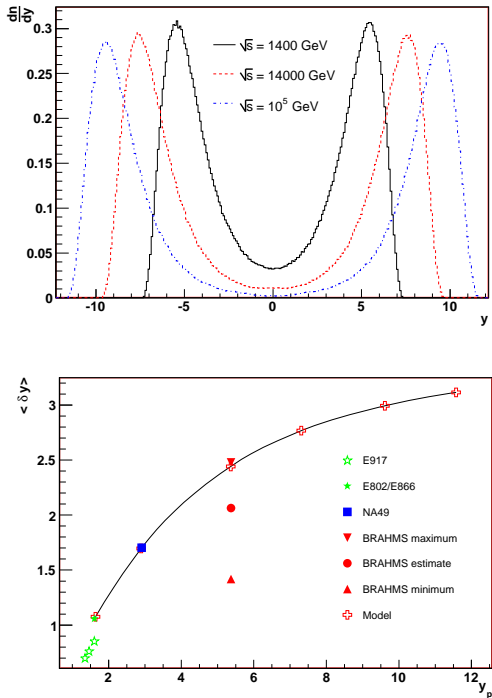


FIG. 11: Predictions of the present model for net-baryon rapidity (upper plot) and rapidity loss (lower plot) including higher energies.

Taking the obtained value of λ_v , the predictions of the present model for net-baryon rapidity and rapidity loss at higher centre-of-mass energies were obtained and

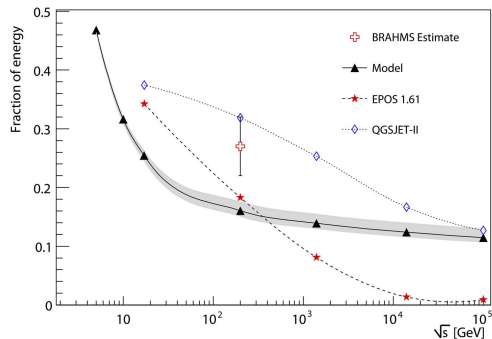


FIG. 12: Evolution of the fraction of energy carried by the Net-Baryon with \sqrt{s} . The prediction of the present model (with a shaded band corresponding to the 1σ variation of the fit parameters) is shown, together with the results obtained with EPOS and QGSJET-II. The data point corresponds to the RHIC estimate given in [23].

are shown in figure 11, covering both the LHC and the high energy cosmic ray regions. In addition, the fraction of the centre-of-mass energy carried by the net-baryon as a function of \sqrt{s} was computed and is shown in figure 12 (together with the 1σ bounds). The predictions of EPOS 1.61 and QGSJET-II.03 are also shown. According to [23], RHIC data point to about 27% of the initial energy remaining in the net-baryon after the collision. This result is also shown in the figure. It is apparent that EPOS, QGSJET-II and the present model show rather different trends. The present model and EPOS agree reasonably well at RHIC energies, where they are both slightly below the measured value. At these energies, QGSJET-II is somewhat above, but equally compatible with data. At higher energies, while in EPOS 1.61 the net-baryon is essentially zero, in the present model and in QGSJET-II.03 a sizable amount of energy is still associated to the net-baryon. It should be noted that high energy effects such as string percolation may change these predictions [26].

V. SUMMARY AND CONCLUSIONS

A simple but consistent model for net-baryon production in high energy hadron-hadron, hadron-nucleus and nucleus-nucleus collisions was presented. The basic ingredients of the model are valence string formation based on standard PDFs with QCD evolution and string fragmentation via the Schwinger mechanism. The results of the model were presented and compared with data from RHIC, SPS and AGS, and with existing models, namely QGSJET-II and EPOS 1.61. The obtained results show that a good description of the main features of net-baryon data is achieved on the basis of this simple model, in which the fundamental production mechanisms appear in a transparent way.

The free parameters in the model, the effective Q^2 and the number of participating nucleons, were fitted to net-baryon data at $\sqrt{s} \simeq 5, 17$ and 200 GeV. A good fit to data is obtained within this model, and the values obtained for the number of participants are in agreement with what we would expect from the literature.

Using the (scarce) net-baryon data at different centre-of-mass energies, a relation between the effective momentum transfer and the centre-of-mass energy was motivated and a prediction was obtained and extrapolated to higher energies for the evolution with \sqrt{s} of the fraction of the initial energy carried away by the net-baryon. A sizable amount of energy may be associated to the net-baryon, even at high energies.

Acknowledgments

We thank K. Werner for kindly providing us the EPOS 1.61 code and for useful discussions and advice on its usage and results. We thank S. Ostapchenko for kindly providing us a QGSJET-II.03 standalone heavy-ion version and for useful discussions. We thank N. Armesto for useful discussions. J. A-M is supported by the “Ramón y Cajal” program, and also by Ministerio de Educación y Ciencia (2004-01198), CICYT (FPA 2005-01963), Xunta de Galicia (2003 PX043, 2005 PXIC20604PN), and Feder Funds, Spain. R. Conceição and J. G. Milhano acknowledge the support of FCT, Fundação para a Ciência e a Tecnologia and Feder Funds, Portugal.

-
- [1] W. Kittel, E.A. De Wolf, “Soft multihadron dynamics”, World Scientific (2005), ISBN 981-256-295-8.
- [2] L. Van Hove, S. Pokorski, Nucl. Phys. B 86 (1975) 245; L. Van Hove, Acta Phys. Pol. B 7 (1976) 339.
- [3] R.P. Feynman, Phys. Rev. Lett. 23 (1969).
- [4] J. Dias de Deus and J.G. Milhano, arXiv:0708.1717 [hep-ph].
- [5] B.B. Back, Phys. Rev. C 72 (2005).
- [6] N.N. Kalmykov, S.S. Ostapchenko, Yad. Fiz. 56 (1993) 105; Phys. At. Nucl. 56 N3 (1993) 346; N.N. Kalmykov, S.S. Ostapchenko, A.I. Pavlov, Izv. RAN Ser. Fiz. 58 (1994) N12 p.21; Bull. Russ. Acad. Science (Physics) 58 (1994) 1966; Nucl. Phys. B (Proc. Suppl.) 52 B (1997) 17.
- [7] S.S. Ostapchenko, Nucl. Phys. B (Proc. Suppl.) 151 (2006) 143 and 147; Phys. Rev. D 74 (2006) 014026; private communications.
- [8] K. Werner, F.M. Liu and T. Pierog, Phys. Rev. C 74 (2006) 044902; K. Werner, private communications.
- [9] R.S. Fletcher, T.K. Gaisser, P. Lipari, T. Stanev, Phys. Rev. D 50 (1994) 5710; J. Engel, T.K. Gaisser, P. Lipari, T. Stanev, Phys. Rev. D 46 (1992) 5013; R. Engel, T.K. Gaisser, P. Lipari, T. Stanev, Proc. 26th ICRC, Salt Lake City (USA), 1 (1999) 415.
- [10] A. Capella, U. Sukhatme, C.-I. Tan, J. Tran Thanh Van, Phys.Rept. 236 (1994) 225-329.
- [11] BRAHMS Collab., I.G. Bearden et. al., Phys. Rev. Lett. 93 (2004) 102301.
- [12] Glauber, R.J. 1959. In Lectures in Theoretical Physics, ed. WE Brittin and LG Dunham, 1:315. New York: Interscience; M.L. Miller, K. Reygiers, S.J. Sanders, P. Steinberg, nucl-ex/0701025.
- [13] E917 Collaboration, B.B. Back et al., Phys. Rev. Lett. 86 (2001) 1970; F. Videbaek and O. Hansen, Phys. Rev. C 52 (1995) 2684; E802 Collab., L. Ahle et al., Phys. Rev. C 60 (1999) 064901; E877 Collab., J. Barette et al., Phys. Rev. C 62 (2000) 024901.
- [14] NA49 Collab., H. Appelshauser et al., Phys. Rev. Lett. 82 (1999) 2471.
- [15] C.E. Aguiar, R. Andrade, F. Grassi, Y. Hama, T. Kodama, T. Osada and O. Socolowski Jr., Brazilian Journal of Physics, Vol. 34, no. 1A (2004) 319.
- [16] S.A. Bass, B. Muller and D.K. Srivastava, Phys. Rev. Lett. 91 (2003) 052302;
- [17] J. Pumplin, D.R. Stump, J.Huston, H.L. Lai, P. Nadolsky, W.K. Tung, JHEP 0207 (2002) 012; D. Stump, J. Huston, J. Pumplin, W.K. Tung, H.L. Lai, S. Kuhlmann, J. Owens, JHEP 0310 (2003) 046; S. Kretzer, H.L. Lai, F. Olness, W.K. Tung, Phys. Rev. D 69(2004) 114005.
- [18] D. Kharzeev, Phys. Lett. B 378 (1996) 238; A. Capella, B.Z. Kopeliovich, Phys. Lett. B 381 (1996) 325; S.E. Vance, M. Gyulassy, X.N. Wang, Phys. Lett. B 443 (1998) 45; S.E. Vance, M. Gyulassy, Phys. Rev. Lett. 83 (1999) 1735.
- [19] G.H. Arakelian, A. Capella, A.B. Kaidalov, Yu.M. Shabelski, Eur. Phys. J. C 26 (2002) 81; F. Bopp, Yu.M. Shabelski, Eur. Phys. J. A 28 (2006) 237.
- [20] B. Andersson, G. Gustafson, T. Sjöstrand, Nucl. Phys. B 197 (1982) 45; B. Andersson, G. Gustafson, T. Sjöstrand, Physica Scripta 32 (1985) 574; P. Edén, G. Gustafson, Z. Phys. C75 (1997) 41.
- [21] K.J. Eskola, V.J. Kolhinen and C.A. Salgado, Eur. Phys. J. C. 9 (1999) 61; K.J. Eskola, V.J. Kolhinen and P.V. Ruuskanen, Nucl. Phys. B 535 (1998) 351.
- [22] D. de Florian, R. Sassot, Phys. Rev. D 69 (2004) 074028.
- [23] B.B. Back, nucl-ex/0508018.
- [24] D. Kharzeev and M. Nardi, nucl-th/0012025.
- [25] V.A. Abramovsky, E.V. Gedalin, E.G. Gurvich, O.V. Kancheli, Sov. J. Nucl. Phys. 53 (1991) 172-176; N.S. Amelin, N. Armesto, C. Pajares, D. Sousa, Eur. Phys. J. C 22 (2001) 149-163.
- [26] J. Alvarez-Muñiz, P. Brogueira, R. Conceição, J. Dias de Deus, M. C. Espírito Santo and M. Pimenta, Astropart. Phys. 27 (2007) 271; J. Dias de Deus, M. C. Espírito Santo, M. Pimenta and C. Pajares, Phys. Rev. Lett. 96 (2006) 162001.